PHYSICAL REVIEW B **85**, 201413(R) (2012)

Minigap isotropy and broken chirality in graphene with periodic corrugation enhanced by cluster superlattices

J. Sánchez-Barriga, A. Varykhalov, D. Marchenko, M. R. Scholz, and O. Rader
Helmholtz-Zentrum Berlin für Materialien und Energie, Elektronenspeicherring BESSY II, Albert-Einstein-Strasse 15, D-12489 Berlin, Germany

(Received 29 February 2012; published 24 May 2012)

The chirality of charge carriers in graphene determines its peculiar scattering properties and in particular the avoided backscattering, predicted to be observable in periodically corrugated graphene as the closing of the so-called minigaps. These are small gaps appearing in the graphene π band at the crossings with umklapp-induced replica bands of the Dirac cone. By angle-resolved photoemission of corrugated graphene on Ir(111), we observe that the minigaps are instead isotropic and close nowhere in **k** space, unexpected for chiral charge carriers. Artificially enhancing the periodic superpotential by deposition of Au and Ir clusters confirms the minigap isotropy, indicating that the origin of this behavior is directly connected to the broken chirality in the system.

DOI: 10.1103/PhysRevB.85.201413 PACS number(s): 73.22.Pr, 73.20.−r, 73.21.Cd, 79.60.−i

The charge carriers in graphene display a linear dispersion as light and neutrinos do. One of the most fascinating aspects of graphene is the absence of backscattering which is derived from the chiral symmetry of electronic states and the way the linear dispersion results from the geometrical structure. Graphene consists of two carbon sublattices A and B which are identified as a pseudospin. The isospin of $\overline{K}$ and $\overline{K}'$ valleys is a conserved quantum number so that electrons that backscatter by 180° would violate this conservation. The linear dispersion has the additional consequence that the group velocity is independent of a potential offset and this enables Klein tunneling through high and wide potential barriers in single-layer graphene.[1–3]

A possible way of adding an extra potential to graphene is to produce corrugated graphene which then results in a superlattice in two dimensions. The superlattice leads to additional mini Brillouin zones (MBZs) in reciprocal space which can be studied by band-structure theory and by angle-resolved photoelectron spectroscopy (ARPES) experiments on appropriate samples. Such is indeed realistic as it was found that already free graphene is corrugated,[4] and this property has since been investigated frequently.[5–8] The fact that Klein tunneling through a potential barrier in graphene requires normal incidence has been employed for electron confinement.[9,10] In corrugated graphene, it introduces an anisotropy in the transport properties. Calculations based on density functional theory reveal for corrugated graphene additional dispersion branches of massless Dirac fermions leading to the generation of extra Dirac points at the boundaries of the MBZs caused by the superlattice.[11–13] The anisotropy, which is due to the chirality of graphene, is revealed as minigaps which open and close depending on the location along the MBZ boundary.[11,12]

In particular, the theoretical analysis by density functional theory of the electronic and transport properties of graphene under periodic potentials has shown that group velocities of charge carriers are strongly direction dependent, being reduced to zero along some directions.[11] The avoided backscattering has been found to occur only along certain directions, as seen from the behavior of the minigaps: In a one-dimensionally corrugated graphene, the minigaps close in the middle of the MBZ boundaries and in two-dimensionally corrugated graphene this occurs both in the middle and at the corners of the boundaries.[11]

From scanning tunneling microscopy (STM) experiments it is known that corrugated graphene can be produced in a controlled way when it is grown on a substrate with large lattice mismatch such as Ru(0001) (Ref. 14) or Ir(111),[15] leading to a moiré superstructure. A large corrugation (i.e., the variation in height between valleys and hills) of ∼0.35 Å was found for graphene on Ir(111),[16] and this system has been studied by ARPES where indeed minigaps have been observed.[17,18] However, no agreement has been reached between Refs. 17 and 18 on the variation of the minigaps along the MBZ boundary, possibly because the minigaps in bare graphene/Ir are rather small (∼0.2 eV). The variation was found to be much smaller than by a factor of ∼2.4 (Ref. 17) and possibly of a reversed trend.[18] Most recently, for Ir cluster superlattices grown on graphene/Ir(111), the renormalization of group velocities due to the additional cluster superpotential has been investigated by ARPES.[19] A strong anisotropy of group velocities was found,[19] in agreement with the theoretical prediction for corrugated graphene of Ref. 11. Although the minigap behavior was not investigated,[19] one may expect it to follow the behavior of the group velocity renormalization along different directions in **k** space.

In the present Rapid Communication we subject the theoretical prediction[11] to a more rigorous experimental verification. To achieve this, we artificially enhance the amplitude of the periodic superpotential by deposition of periodic Au and Ir clusters on graphene/Ir(111). Using high-resolution ARPES, we reinvestigate the asymmetry of group velocities and scrutinize the behavior of the minigaps and their expected periodic closure along the MBZ boundaries. We find that the minigap size is largely increased (by a factor of ∼2) and observe the expected periodic change of the binding energy of the minigaps. However, at odds with theory, we show that pure graphene on Ir exhibits a clear isotropy in the minigap size and that the twice larger minigaps due to the enhancement of the periodic potential by clusters are isotropic as well.

ARPES measurements were conducted at 30 K and at room temperature (RT) in ultrahigh vacuum better than

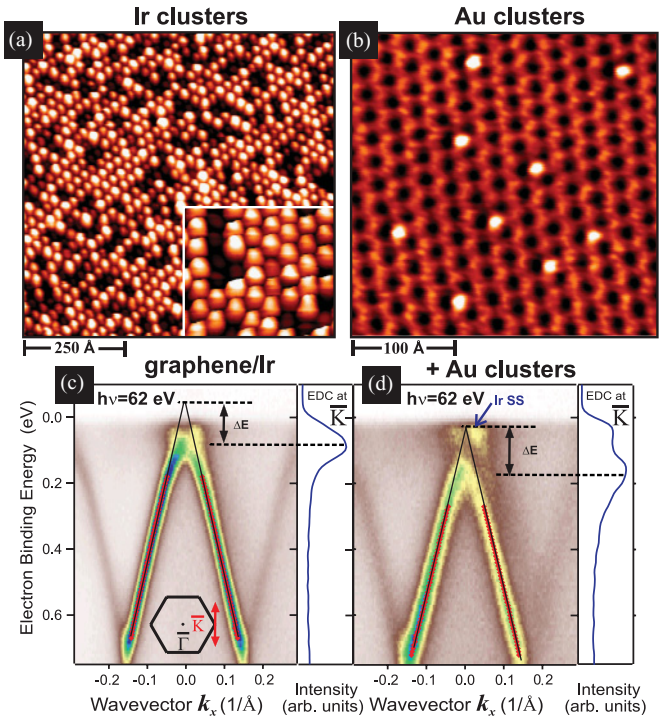

FIG. 1. (Color online) (a), (b) STM images of Ir (a) and Au (b) clusters grown on moiré-patterned graphene/Ir(111). Tunneling parameters were $V_t = +1.6$ V, $I_t = 0.5$ nA in (a) and $V_t = +0.03$ V, $I_t = 6$ nA in (b). Inset in (a): High-resolution STM from Ir clusters revealing their hexagonal shape. (c), (d) Dirac cones measured by ARPES before (c) and after (d) deposition of 0.1 ML of Au. Red (light) points are fits to the peak positions, and black (dark) lines fits to the linear part of the dispersion. Inset in (c): The experimental geometry. Right panels: Spectra at $\overline{K}$.

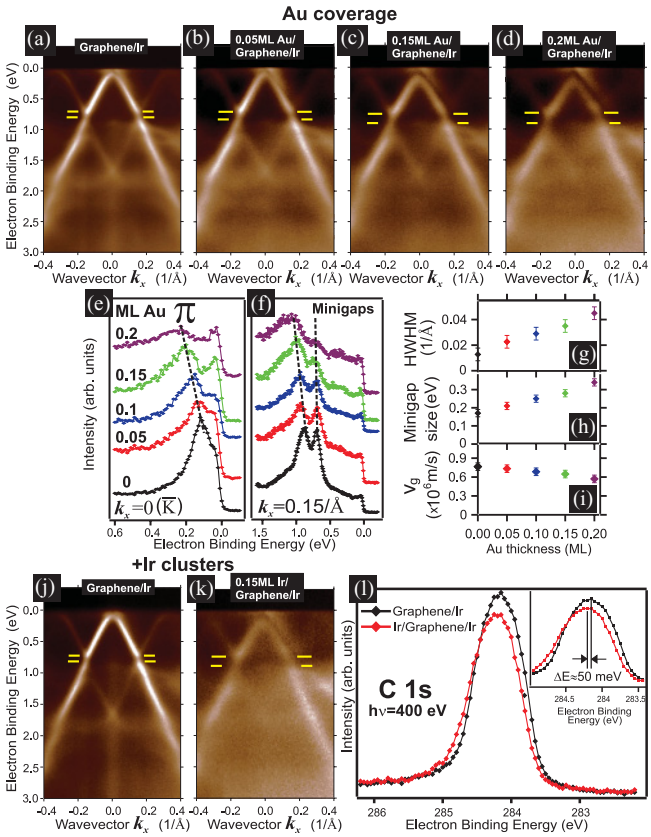

FIG. 2. (Color online) (a)–(d) Evolution of asymmetric Dirac cones with coverage of Au clusters at low temperature. Minigaps are highlighted with horizontal yellow (light) lines. Spectra at (e) $\overline{K}$ point and (f) $k = 0.15$ Å^{-1} emphasize the progressive opening of a gap at the Dirac point and the enlargement of the minigap size, respectively. (g) Change in the linewidth, (h) minigap size, and (i) group velocity v_g induced by the clusters. (j), (k) Dirac cones measured at RT for (j) graphene/Ir and (k) after deposition of 0.15 ML Ir clusters on top. (l) C 1s core levels measured at $h\nu = 400$ eV before [black (dark) symbols] and after [red (light) symbols] cluster growth. Inset: Zoom on the C 1s peak showing a shift of 50 meV.

1×10^{-10} mbar with the ARPES 1^2 end station at the UE112-PGM2 beamline of BESSY II using p-polarized light. STM data have been acquired with an Omicron VT STM instrument at RT. The clean Ir(111) surface and the graphene layer were prepared following identical procedures described elsewhere.[20] Subsequent growth of Au or Ir clusters was performed *in situ* at low and RT, respectively, at a flux rate of ~0.01 monolayer (ML)/min.

Figure 1 shows our STM characterization of Ir [Fig. 1(a)] and Au [Fig. 1(b)] clusters grown on graphene on Ir(111). It demonstrates that both Au and Ir clusters are periodic and can be stabilized on top of the graphene moiré at RT. The deposited Ir keeps decorating the moiré superstructure at even high nominal concentrations of up to 3 ML [Fig. 1(a)]. The Ir clusters exhibit uniform dimensions and a very periodic arrangement, with a periodicity of ~25 Å in registry with the moiré superstructure. The same is true for Au clusters, but at RT only small individual clusters remain stable at very low Au concentrations of about 0.3 ML [Fig. 1(b)]. In agreement with earlier studies,[21] we find that growth and ARPES characterization of periodic and larger Au clusters requires low temperature of the substrate.

We will first discuss the modification induced by the external cluster superpotential on the graphene electronic structure, which is shown in Figs. 1(c), 1(d), and 2. We emphasize that we do not observe large differences in the behavior of the Dirac cone in graphene on Ir(111) upon deposition of Au or Ir clusters. The measurements have been performed with a photon energy $h\nu = 62$ eV and $\mathbf{k}$ perpendicular to the $\overline{\Gamma K}$ direction ($\perp \overline{\Gamma K}$) of the graphene surface Brillouin zone [see the inset in Fig. 1(c)]. Figures 1(c) and 1(d) show the ARPES intensity near the Fermi level (E_F, i.e., zero binding energy) of the graphene π band forming a Dirac cone before and after deposition of 0.1 ML Au, respectively. A shift of the π-band summit to higher binding energy is clearly observed. Figure 2 reveals further how the Dirac cone is progressively modified with increasing Au cluster thickness at low temperature. Similar results were obtained for Ir clusters at RT [see Figs. 2(j) and 2(k)]. The Dirac cone is subject to diffraction effects induced by the moiré superlattice, and minigaps appear at the crossings of umklapp-induced replicas of the π band.[17] In agreement with recent studies,[19] the deposition of clusters increases the energy size of the minigaps [see Figs. 2(a)–2(d), the spectra in Fig. 2(f), and the values in Fig. 2(h)]. Furthermore, it can be seen in Fig. 2 how π-band intensity [Fig. 2(f)] and quasiparticle lifetimes

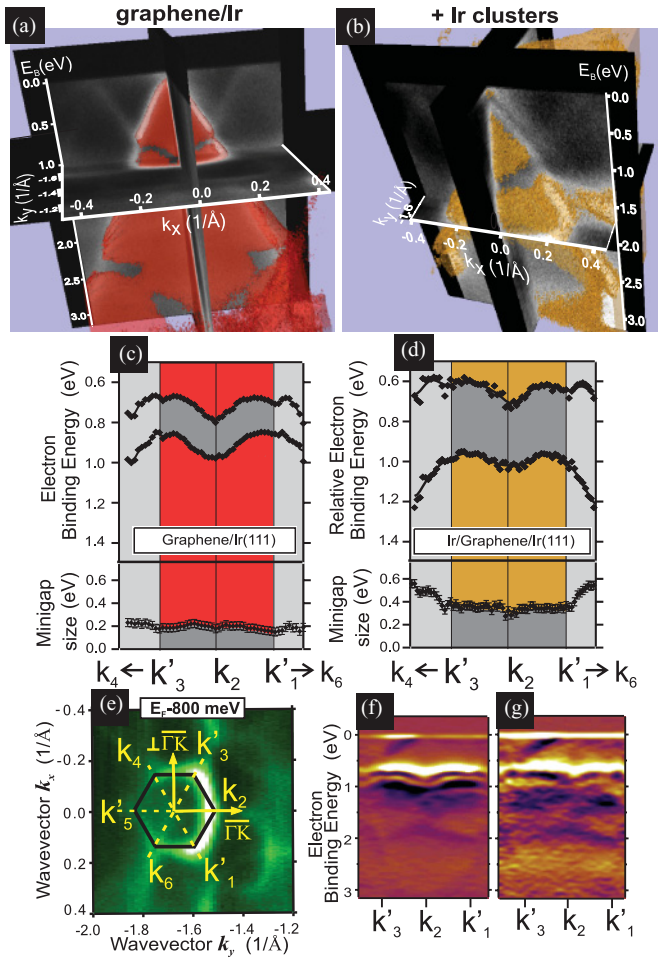

FIG. 3. (Color online) Tomographic view of Dirac cones (a) before and (b) after Ir cluster deposition. Photoemission intensity appears as a color pixel when it reaches a threshold value. The threshold is fixed for the entire figure. (c), (d) Top: Corresponding minigap dispersions; bottom: minigap sizes. (e) Constant energy cut of graphene/Ir near the binding energy of the minigaps ($h\nu = 62$ eV). A scheme of the graphene MBZ is on top (black lines). (f), (g) First derivative of the ARPES intensity in the region of minigaps. (a), (c), (f) Before and (b), (d), (g) after growth of 0.15 ML Ir clusters.

[Fig. 2(g)] are strongly reduced due to extra scattering effects induced by the clusters and group velocities v_g [Fig. 2(i)] are renormalized, in qualitative agreement with the theoretical prediction.[11] Comparing the size of these effects before and after deposition of 0.2 ML Au leads us to the following results: (i) The half-width at half maximum (HWHM) [as extracted from fits to momentum distribution curves (MDCs)] increases from ∼0.0128 to ∼0.045 Å^{-1}, (ii) minigaps can be tuned and are enlarged from (170 ± 10) meV to (350 ± 20) meV, and (iii) due to group velocity renormalization, v_g changes from $\sim(0.77 \pm 0.01) \times 10^6$ to $\sim(0.56 \pm 0.02) \times 10^6$ m/s. For graphene on Ir, v_g is closest to the theoretical value of $v_g = 0.8 \times 10^6$ m/s from tight binding calculations for freestanding graphene,[22,23] but is reduced by a factor of ∼1.4 due to the external potential exerted by the clusters.

Most intriguing is the isotropic behavior of the minigaps in **k** space, reported in Fig. 3 for graphene/Ir and Ir/graphene/Ir systems. We have observed a similar behavior for Au clusters. The above mentioned effects and, in particular, the minigap isotropy, can already be seen well in tomographic views of the Dirac cones before [Fig. 3(a)] and after [Fig. 3(b)] Ir deposition. Other gaps at high binding energies (∼2.5 eV) and larger in size (∼0.7 eV) can also be observed. The minigaps at low binding energy [Figs. 3(c) and 3(d)] have been extracted along the MBZ [Fig. 3(e)] from precise fits to the ARPES intensity [Figs. 3(f) and 3(g)]. For graphene/Ir, we find a constant minigap size of ∼170 meV in the full MBZ. We do not observe the reported increase to ∼230 meV beyond the k_3' and k_1' points.[18] However, the effect from the Ir cluster superpotential preserves the minigap isotropy to a constant value of ∼350 meV along the k_3'-k_2'-k_1' line. It increases only beyond these points, reaching up to ∼590 meV. This increase is not a property of the graphene but due to the presence of Ir bands which do not possess the full symmetry of the graphene superlattice. For both the moiré superpotential with and without external enhancement, the periodic change in the binding energy of the upper and lower bands around the minigaps qualitatively agrees with the theoretical prediction.[11] But this does not hold for the dependence of the minigap size we observe between k_3' and k_1' points, because minigap closure should occur in the MBZ boundaries exactly in the middle between $k_2$and k_1' points and k_2 and k_3' points due to the chiral nature of graphene states.[11] It has been confirmed that the closing of the minigaps disappears and a behavior such as the one measured here occurs exactly when the chirality in graphene is broken.[11] Therefore, we conclude that the absence of minigap closure must be directly connected to a loss of chirality in graphene states which intermixes π states at $\overline{K}$ and $\overline{K}'$. But this connection does not hold for the gaps at ∼2.5 eV because they are of a different nature than the minigaps. This is demonstrated in Fig. 4(a), where the full dispersion of the graphene π band for pure graphene/Ir along the $\overline{\Gamma K}$ direction is shown. We clearly observe that these gaps are not due to crossings with replica π bands as recently suggested[24] but to hybridization with flat d bands from the Ir substrate. As a result, avoided-crossing effects in the graphene π band which lead to the formation of these hybridization gaps are clearly observed.

The origin of the broken chirality in graphene states can be further studied by the intensity distribution of the π band and its replicas. Constant-energy maps should be anisotropic if the A-B sublattice symmetry remains intact,[25,26] but this is not the case for graphene/Ir [Fig. 4(b)] and 0.2 ML Au/graphene/Ir [Fig. 4(c)]. (The very intense structures are due to the Ir.) This means that A-B sublattice symmetry is broken, which is likely the cause of the loss in chirality. As the A-B symmetry breaking interaction, we identify first of all the one with the Ir substrate: The corrugation means a periodically closer contact to the substrate. The local adsorption is such that graphene sublattice A is sitting on top of the topmost Ir atoms while sublattice B sits on hollow sites. Cluster adsorption enhances this effect as it decreases the graphene-Ir distance further.[15] It should be mentioned that also the replica bands show sixfold symmetry in their intensities, which differs from previous results.[19]

We want to make the connection to the recent finding of a large anisotropy of v_g which appears to be in contrast to the

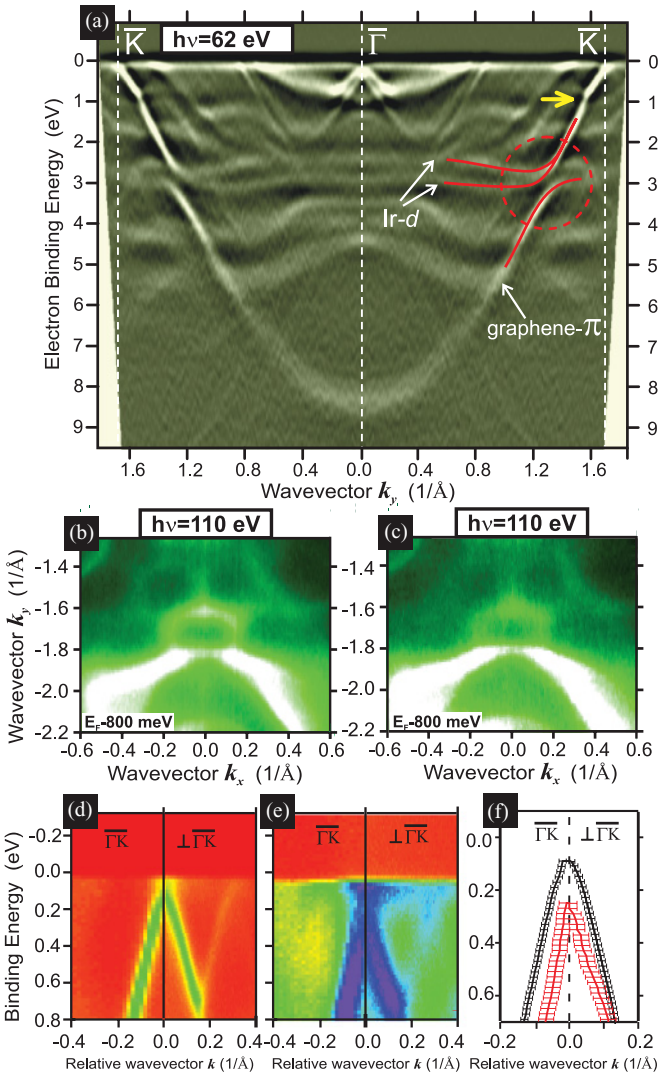

FIG. 4. (Color online) (a) Second derivative of the ARPES intensity showing dispersion acquired for bare graphene/Ir(111) along the $\overline{\Gamma K}$ direction (data is symmetrized). Red continuous lines show the dispersion of the bands and a typical avoided-crossing effect. The red (light) dashed circle emphasizes the position of the hybridization gap. The top arrow indicates the minigap at lower binding energy. (b)–(e) π-band constant energy maps (b) before and (c) after Au deposition. Observation of asymmetric Dirac cones in (d) graphene on Ir(111) and (e) with 0.2 ML Au clusters grown on top. (f) Dispersions of the π band extracted by fitting ARPES data shown in (d) [black (dark)] and (e) [red (light)]. Error bars are the peak widths obtained from fits to MDCs.

present finding of isotropy of the minigaps. The anisotropy of v_g can be noticed best when comparing the π-band linear dispersions along $\overline{\Gamma K}$ and $\perp\overline{\Gamma K}$ to each other as is done in Figs. 4(d)–4(f). From fits to MDCs [Fig. 4(f)], we find that $v_{g,||} = (0.85 \pm 0.01) \times 10^6$ m/s is almost not renormalized, leading to an anisotropy $(v_{g,||} - v_{g,\perp})/v_{g,\perp} = (11 \pm 3)\%$ for graphene on Ir which increases up to $(50 \pm 6)\%$ after cluster deposition. This is mainly due to different sizes of the MBZ along $\overline{\Gamma K}$ and $\perp\overline{\Gamma K}$ which becomes increasingly more important when the growing and isotropic minigap reduces the width of the miniband. In particular, such an anisotropy cannot be due to a reduced symmetry of the cluster superpotential, as recently proposed,[19] because it remains sixfold. Therefore, only the isotropic enlargement of the minigaps is the reason for changes in the group velocity renormalization. Since a smaller group velocity renormalization can occur for enlarged minigaps at high binding energy, we attribute the observed anisotropic behavior to the strong periodic dependence of the minigap binding energy within the full MBZ.

Because the existence of a broken chirality seems to be a consequence of sublattice symmetry breaking, not less important is to know if there is a gap at $\overline{K}$ in graphene on Ir and to find out why the π band seen in Figs. 1(d) and 2(b)–2(e) shifts upon deposition of Au. Note that the minigaps shift to higher binding energy as well [see Fig. 2(f)]. Because the ARPES spectra do not reveal the unoccupied π^* band located above E_F, it is not clear *a priori* if such a shift is only due to charge doping effects,[27] due to sublattice symmetry breaking in graphene meaning an enlarged band gap at the $\overline{K}$ point,[25,28] or to a combination of both. We have, therefore, precisely fitted the linear part of the band dispersions [see Figs. 1(c) and 1(d)] and performed C 1*s* core-level photoemission experiments to reveal the doping contribution [see Fig. 2(l) and the inset]. We also notice that after cluster deposition the C 1*s* core level does not become strongly asymmetric, in contrast to recent studies.[29] Our results are consistent with a weak or almost absent sp_2 to sp_3 graphene rehybridization of C atoms below the clusters, at least for the relatively small cluster thicknesses we have investigated. For graphene/Ir [Fig. 1(c)], we find that the Dirac point is located above E_F at a binding energy of $E_D \sim (-35 \pm 15)$ meV and the π-band summit at $E_\pi \sim (80 \pm 10)$ meV. This corresponds to an existing energy gap at the $\overline{K}$ point larger than $2\Delta E = (230 \pm 15)$ meV, consistent with sublattice symmetry breaking in graphene. Note that an Ir surface state band[17] relatively mimicked under the π-band summit in Fig. 1(c) becomes visible in Fig. 1(d) after Au deposition. Because we do not find clear signs of hybridization of this band with graphene π states, we argue that hybridization effects with Ir states are not the reason for the enlargement of the band gap, as recently suggested.[18] For the largest cluster superpotential amplitudes (~0.2 ML Au and ~0.15 ML Ir), we obtain $E_D \sim (15 \pm 20)$ meV and $E_\pi \sim (190 \pm 10)$ meV. This means a total shift of the π-band summit of $\Delta E_\pi \sim (110 \pm 20)$ meV and a shift of the Dirac point by $\Delta E_D \sim (50 \pm 20)$ meV revealing the charge doping contribution, both consistent with a tunable band gap larger than $2\Delta E \sim (350 \pm 20)$ meV. Therefore, the deposition of clusters enlarges the band gap at $\overline{K}$, meaning an enhanced sublattice symmetry breaking in graphene. We conclude that this gives rise to a broken chirality in the system which leads to extra intervalley scattering between the $\overline{K}$ and $\overline{K}'$ points and preserves the minigap isotropy, opening up a unique tunable backscattering channel which suppresses Klein tunneling.

In summary, we have investigated the electronic band structure of graphene on Ir(111) under the effect of cluster superpotentials of different sizes. We have examined the asymmetry of group velocities and in particular the behavior

of the minigaps and their preditced periodic closure along the MBZ boundaries. We observe an unexpected minigap isotropy which remains unaffected by enhancing the amplitude of the superlattice potential. We conclude that the origin of this behavior is the broken chirality in the system. The strong anisotropy of the group velocity is consistent with this and results very simply from the Brillouin zone geometry.

This work was supported by SPP 1459 of the Deutsche Forschungsgemeinschaft.

[1] M. I. Katsnelson, K. S. Novoselov, and A. K. Geim, Nat. Phys. **2**, 620 (2006).
[2] V. V. Cheianov and V. I. Fal'ko, Phys. Rev. B **74**, 041403(R) (2006).
[3] T. Ando, T. Nakanishi, and R. Saito, J. Phys. Soc. Jpn. **67**, 2857 (1998).
[4] J. C. Meyer, A. K. Geim, M. I. Katsnelson, K. S. Novoselov, T. J. Booth, and S. Roth, Nature (London) **446**, 60 (2007).
[5] L. Brey and J. J. Palacios, Phys. Rev. B **77**, 041403(R) (2008).
[6] F. Guinea, M. I. Katsnelson, and M. A. H. Vozmediano, Phys. Rev. B **77**, 075422 (2008).
[7] I. F. Herbut, V. Juričić, and O. Vafek, Phys. Rev. Lett. **100**, 046403 (2008).
[8] A. Cortijo and M. A. H. Vozmediano, Phys. Rev. B **79**, 184205 (2009).
[9] P. G. Silvestrov and K. B. Efetov, Phys. Rev. Lett. **98**, 016802 (2007).
[10] J. H. Bardarson, M. Titov, and P. W. Brouwer, Phys. Rev. Lett. **102**, 226803 (2009).
[11] C.-H. Park, L. Yang, Y.-W. Son, M. L. Cohen, and S. G. Louie, Nat. Phys. **4**, 213 (2008); Phys. Rev. Lett. **101**, 126804 (2008).
[12] C.-H. Park, Y.-W. Son, L. Yang, M. L. Cohen, and S. G. Louie, Phys. Rev. Lett. **103**, 046808 (2009).
[13] L. Brey and H. A. Fertig, Phys. Rev. Lett. **103**, 046809 (2009).
[14] S. Marchini, S. Günther, and J. Wintterlin, Phys. Rev. B **76**, 075429 (2007).
[15] A. T. N'Diaye, S. Bleikamp, P. J. Feibelman, and T. Michely, Phys. Rev. Lett. **97**, 215501 (2006).
[16] C. Busse *et al.*, Phys. Rev. Lett. **107**, 036101 (2011).
[17] I. Pletikosić, M. Kralj, P. Pervan, R. Brako, J. Coraux, A. T. N'Diaye, C. Busse, and T. Michely, Phys. Rev. Lett. **102**, 056808 (2009).
[18] E. Starodub, A. Bostwick, L. Moreschini, S. Nie, F. E. Gabaly, K. F. McCarty, and E. Rotenberg, Phys. Rev. B **83**, 125428 (2011).
[19] S. Rusponi, M. Papagno, P. Moras, S. Vlaic, M. Etzkorn, P. M. Sheverdyaeva, D. Pacilé, H. Brune, and C. Carbone, Phys. Rev. Lett. **105**, 246803 (2010).
[20] A. Varykhalov, D. Marchenko, M. R. Scholz, E. D. L. Rienks, T. K. Kim, G. Bihlmayer, J. Sánchez-Barriga, and O. Rader, Phys. Rev. Lett. **108**, 066804 (2012).
[21] A. T. N'Diaye, T. Gerber, C. Busse, J. Mysliveček, J. Coraux, and T. Michely, New J. Phys. **11**, 103045 (2009).
[22] S. Reich, J. Maultzsch, C. Thomsen, and P. Ordejón, Phys. Rev. B **66**, 035412 (2002).
[23] P. R. Wallace, Phys. Rev. B **71**, 622 (1947).
[24] M. Kralj, I. Pletikosić, M. Petrović, P. Pervan, M. Milun, A. T. N'Diaye, C. Busse, T. Michely, J. Fujii, and I. Vobornik, Phys. Rev. B **84**, 075427 (2011).
[25] A. Bostwick, T. Ohta, J. L. McChesney, K. V. Emtsev, T. Seyller, K. Horn, and E. Rotenberg, New J. Phys. **9**, 385 (2007).
[26] M. Mucha-Kruczyński, O. Tsyplyatyev, A. Grishin, E. McCann, V. I. Fal'ko, A. Bostwick, and E. Rotenberg, Phys. Rev. B **77**, 195403 (2008).
[27] A. Varykhalov, M. R. Scholz, T. K. Kim, and O. Rader, Rev. B **82**, 121101(R) (2010).
[28] R. Balog *et al.*, Nat. Mater. **9**, 315 (2010).
[29] J. Knudsen, P. J. Feibelman, T. Gerber, E. Grånäs, K. Schulte, P. Stratmann, J. N. Andersen, and T. Michely, Phys. Rev. B **85**, 035407 (2012).